The International Journal of Robotics Research
http://ijr.sagepub.com/

Wearable soft sensing suit for human gait measurement

Yigit Mengüç, Yong-Lae Park, Hao Pei, Daniel Vogt, Patrick M. Aubin, Ethan Winchell, Lowell Fluke, Leia Stirling, Robert J. Wood and Conor J. Walsh

The International Journal of Robotics Research 2014 33: 1748 originally published online 13 November 2014
DOI: 10.1177/0278364914543793

The online version of this article can be found at:
http://ijr.sagepub.com/content/33/14/1748

Published by:
SAGE
http://www.sagepublications.com

On behalf of:
ijrr

Multimedia Archives

Article

The International Journal of Robotics Research
2014, Vol. 33(14) 1748–1764

DOI: 10.1177/0278364914543793
ijr.sagepub.com
SAGE

Wearable soft sensing suit for human gait measurement

Yiğit Mengüç[1,2], Yong-Lae Park[3], Hao Pei[1,2], Daniel Vogt[1,2], Patrick M. Aubin[1,2], Ethan Winchell[1], Lowell Fluke[1], Leia Stirling[4], Robert J. Wood[1,2] and Conor J. Walsh[1,2]

Abstract

Wearable robots based on soft materials will augment mobility and performance of the host without restricting natural kinematics. Such wearable robots will need soft sensors to monitor the movement of the wearer and robot outside the lab. Until now wearable soft sensors have not demonstrated significant mechanical robustness nor been systematically characterized for human motion studies of walking and running. Here, we present the design and systematic characterization of a soft sensing suit for monitoring hip, knee, and ankle sagittal plane joint angles. We used hyper-elastic strain sensors based on microchannels of liquid metal embedded within elastomer, but refined their design with the use of discretized stiffness gradients to improve mechanical durability. We found that these robust sensors could stretch up to 396% of their original lengths, would restrict the wearer by less than 0.17% of any given joint's torque, had gauge factor sensitivities of greater than 2.2, and exhibited less than 2% change in electromechanical specifications through 1500 cycles of loading–unloading. We also evaluated the accuracy and variability of the soft sensing suit by comparing it with joint angle data obtained through optical motion capture. The sensing suit had root mean square (RMS) errors of less than 5° for a walking speed of 0.89 m/s and reached a maximum RMS error of 15° for a running speed of 2.7 m/s. Despite the deviation of absolute measure, the relative repeatability of the sensing suit's joint angle measurements were statistically equivalent to that of optical motion capture at all speeds. We anticipate that wearable soft sensing will also have applications beyond wearable robotics, such as in medical diagnostics and in human–computer interaction.

Keywords

Soft sensors, soft robotics, wearable robotics, wearable electronics, motion capture

1. Introduction

With the emergence of soft robotics research there has been a focus on wearable robots that can intimately interface to the wearer, allowing them to maintain natural movement patterns. We have seen an evolution from rigid exoskeletons with rigid actuators (Yagn, 1890; Makinson, 1971; Kawamoto et al., 2003; Pratt et al., 2004; Guizzo and Goldstein, 2005; Kazerooni and Steger, 2006; Walsh et al., 2007) to rigid exoskeletons with soft pneumatic actuators (Yamamoto et al., 2003; Tsuji et al., 2013). In parallel, we have seen soft exosuits with rigid tendon-drive actuators (Galiana et al., 2012; Asbeck et al., 2013) transition to soft exosuits with soft pneumatic actuators (Park et al., 2014; Goldfield et al., 2012; Wehner et al., 2013). However, the use of soft materials presents design and fabrication challenges in the fundamental robotic technologies available for actuation, sensing, and control. To specifically address the sensing challenge, here we present the design, fabrication, and characterization of a soft sensing suit that uses hyperelastic strain sensors and is capable of monitoring the motion of the human body (Figure 1).

Interfacing electronics to biological tissue has gathered a great deal of interest thanks to new technologies that are so thin that they can conform to human skin (Kim et al., 2011), the brain (Viventi et al., 2011), and the heart (Kim

[1]School of Engineering and Applied Sciences, Harvard University, Cambridge, MA, USA
[2]Wyss Institute for Biologically Inspired Engineering at Harvard University, Boston, MA, USA
[3]Robotics Institute, Carnegie Mellon University, Pittsburgh, PA, USA
[4]Department of Aeronautics and Astronautics, Massachusetts Institute of Technology, Cambridge, MA, USA

Corresponding author:
Conor J. Walsh, School of Engineering and Applied Sciences, Harvard University, 60 Oxford Street, Room 409, Cambridge, MA 02138, USA.
Email: walsh@seas.harvard.edu

Fig. 1. Soft strain sensors were placed at each lower limb joint to capture motion in the sagittal plane. In the case of the knee and ankle sensors (insets on left) webbing directed motion over the joint.

et al., 2012). The major approaches to fabricating such flexible electronics are either thin film processing of silicon or organic semiconducting polymers (Rogers et al., 2010). From an actuation perspective, there have historically been many soft approaches including pneumatic actuators (Shulte Jr., 1961; Park et al., 2014; Wehner et al., 2013), wearable tendon-drive actuation (Kong and Jeon, 2006; Galiana et al., 2012; Asbeck et al., 2013), and even soft electroactive polymer actuators (Bar-cohen, 2004), all of which complement the work on sensors we present here. There are many exciting applications for soft wearable robotic systems, such as active orthotics that can monitor a patient's gait pathology and provide the appropriate actuation assistance for rehabilitation (Yifan and Hsiao-Wecksler, 2013), and systems for the able-bodied that can augment human performance by reducing the work required from biological muscles (Asbeck et al., 2013; Park et al., 2014). Apart from their utility in wearable robotic systems, soft sensor technologies will also provide the ability to non-invasively monitor the motion of impaired and healthy individuals in unrestricted settings (De Rossi and Veltink, 2010; Cavallo et al., 2013; Mengüç et al., 2013).

A critical requirement for sensors in soft wearable systems is that they must conform to the body's geometry and soft tissue without impeding the body's natural and nonlinear motions (De Rossi and Veltink, 2010). The gold standard for human motion analysis is optical tracking of passive retroreflective or active markers positioned at key bony landmarks (Zhou and Hu, 2008). Visual tracking provides a means for precise and accurate measurement but is constrained to a fixed sensing volume and requires significant post-processing and kinematic model development.

An alternative approach is to place non-visual sensors directly on the body to eliminate sensing volume constraints. A common approach to body-worn sensors is through the use of inertial measurement units (IMUs) (Giansanti et al., 2003; Luinge and Veltink, 2005), but these sensors require extensive filtering (Yun and Bachmann, 2006) or sensor fusion with external systems (Tao et al., 2007) to eliminate integration drift (Corke et al., 2007).

Another approach is the use of sensors that measure displacement of the body directly, such as with fiber-optic (Wise et al., 1990) and strain-gauge goniometers (Legnani et al., 2000), both of which are inextensible. The latter approach is the most computationally light and most suitable for direct real-time feedback for robot control systems. However, these existing solutions suffer from poor mechanical interfacing to the body due to the sensors' stiff materials.

There are several previous approaches to making soft sensors for measuring displacements of and forces on the body. Prior work on elastomeric sensors approaching skin-like compliance (modulus $<$ 1 MPa) include pressure sensing, strain sensing, and other biometric sensing. Waveguides within rubber were used to create pressure sensors capable of uniaxial strains up to 50% and bending radius of curvature down to 5 mm (Ramuz et al., 2012). Aligned carbon nanotubes (Yamada et al., 2011) and spray-deposited carbon nanotubes (Lipomi et al., 2011) encapsulated in silicone rubber were used to detect gross motion of the leg, finger and throat with hundreds of percent strain. Elastic yarn coated with carbon nanotubes were used to detect strains as large as 30% in limited motion analysis (Zhang et al., 2012). Thin films of silicon encapsulated in soft polymers have been used as electromyographs (Kim et al., 2011) and could withstand strains as high as 40%. Graphite doped rubbers applied as a film on a full-body garment (Tesconi et al., 2007) or glove (Tognetti et al., 2006) demonstrated motion tracking and could be improved with optimized sensor placement (Bianchi et al., 2013a) and optimized estimation techniques based on common human hand kinematics (Bianchi et al., 2013b). These previous devices each have exciting potential uses, but none demonstrated significant mechanical robustness or systematic use for human motion tracking in walking and running.

Our solution to soft sensing is to embed liquid metal microfluidic channels within elastomers. Previously, this technology had been used to measure pressure (Park et al., 2010), strain, and bending (Majidi et al., 2011). By combining sensing modes, sensors could measure pressure and in-plane shear (Vogt et al., 2013) or pressure and in-plane strain (Park et al., 2012). To demonstrate alternative, biocompatible conductive fluidics, a saline–glycerol solution replaced the embedded liquid metal, resulting in a higher resistance, a higher gauge factor, and slightly increased complexity due to use of AC electronics (Chossat et al., 2013). The principle of operation in each case relies on how forces and motions deform the embedded microchannels, thus altering the electrical resistance path along the conductive liquid 'wires' (Park et al., 2012). The design of the elastomeric mechanisms and microchannel paths could also yield different sensing modes. The applications of the sensors were demonstrated for use on fingers (Kramer et al., 2011) and ankles (Park et al., 2011, 2014); however, sensor robustness, integration to garments, and systematic human motion studies were not evaluated.

In this work, we extend the capabilities of our liquid metal embedded within elastomer sensors beyond our previous demonstration of wearable sensing application (Mengüç et al., 2013). The wearable suit in this work, as in Mengüç et al. (2013), measures leg joint angles in the sagittal plane, but now with both legs fully instrumented and validated on multiple participants and at increased locomotion speeds. The current work also introduces new materials and designs to the sensors to improve their mechanical robustness, and ease of attachment and detachment to a generic piece of clothing. We present an overview of the complete sensing system, including the garment, electronics, and sensors along with their design, fabrication, and characterization. The mechanical and electrical behaviors of the sensor were specifically characterized to demonstrate their usefulness and readiness for inclusion in wearable systems. Finally, we compare results of the sensor's performance versus standard motion capture capabilities on three participants during walking and running trials.

2. System description

The wearable soft sensing suit encompasses three components: (1) running tights and shoe insoles which serve as the garment base; (2) custom electronics which collect, amplify, and transmit sensor signals; and (3) the six soft strain sensors created from liquid metal embedded in an elastomer. The strain sensors were arranged as follows to measure sagittal plane joint angles:

- two strain sensors to measure hip angles, one placed dorsally on each gluteus;
- two strain sensors to measure knee angle, one placed frontally on each thigh with inextensible webbing routed across the knee to the shin;
- two strain sensors to measure ankle angle, one placed dorsally on each calf with inextensible webbing routed across the heel to a shoe insole beneath the foot.

2.1. Garment base

Generic running tights were modified with hook-and-loop fasteners which served as anchor points for the strain sensors (Figure 1). Shoe insoles were also modified with the addition of webbing and hook-and-loop attachment points. The pair of elastic running tights were chosen as the garment base layer and the sensor attachment was designed so it could easily be worn under a layer of clothing if required. Hook-and-loop (Loop 3008 type, Velcro USA Inc., Manchester, NH, USA) was cut into patches and sewn to appropriate positions (Figure 1). Sensors were attached to flexible nylon straps, to avoid being placed on the bony landmarks since the soft sensors were sensitive to surface pressure. The nylon's much higher elastic modulus (e.g. 4 GPa) than that of our sensor material (30 kPa for Ecoflex 0030) guaranteed transmission of nearly all of the strain of the joint directly to the sensor.

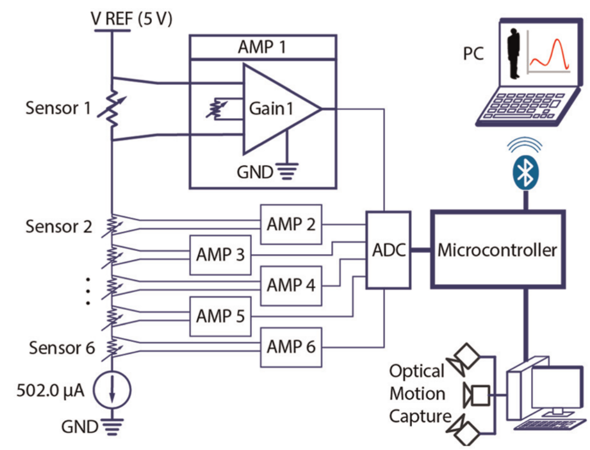

Fig. 2. The six sensors were amplified separately before passing through an analog to digital converter (ADC) on the microcontroller. A Bluetooth communications chip on the microcontroller transmitted the sensor data wirelessly to a PC for data processing and visualization.

2.2. Electronics

The custom electronics consisted of a shield board with amplifier circuits for each of the six sensors, a Bluetooth module, and a microcontroller (Figure 2). The soft sensors' behavior under strain was that of variable resistors. The nominal sensor resistance was near 2.5 Ω and increased up to 15 Ω when stretched by 200%. The amplifier circuit operated at the microcontroller's native reference voltage of 5 V. The circuit applied a precise 502.0 μA DC current through the sensor and then amplified the voltage drop across the sensor resistance through an operational amplifier, which resulted in a linear output voltage to input resistance relationship.

Once amplified, the sensor signal was passed to an Arduino microcontroller (Arduino Mega 2560, Italy) through the on-board analog to digital converter (ADC). A Bluetooth wireless modem (BlueSMiRF Gold, Sparkfun Electronics, USA) transmitted the collected sensor signals to a laptop at up to 135 Hz. Custom MATLAB code on the laptop read the serially transmitted data to produce an

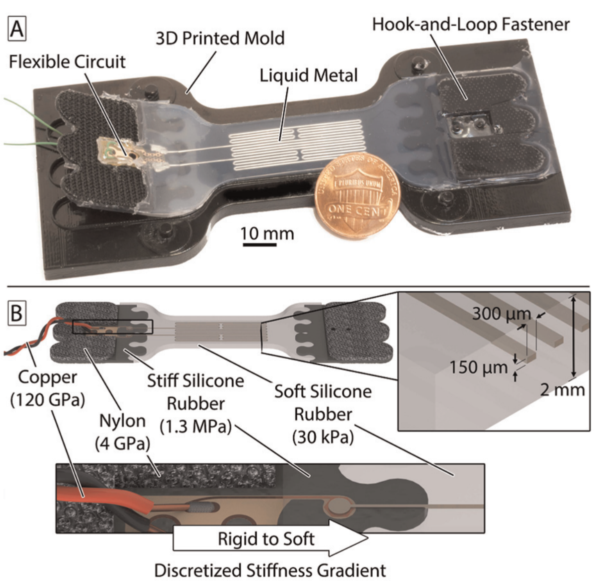

Fig. 3. (A) A photograph of an ankle sensor, with its 3D printed mold, flexible circuit, liquid metal, and hook-and-loop fastener components highlighted. (B) A rendered schematic of an ankle sensor with cross-sectional views revealing the channel geometry (150 μm $\times$ 300 μm) and the discretized stiffness gradient of the four included material types (with their Young's modulus values in parentheses).

animated visual representation of the human (15 Hz refresh rate) while recording the data to file at the maximum 135 Hz for post-processing and characterization. An additional direct wire connection between the microcontroller and optical motion capture system was used to synchronize the start and stop of data collection.

2.3. Soft strain sensor

The soft strain sensors were created out of liquid metal embedded in elastomers and were based on previous work in the Wood lab demonstrated in Park et al. (2010), Majidi et al. (2011), and Kramer et al. (2011). The current sensor design expands on our previous work in Mengüç et al. (2013) which introduced embedded printed circuit boards, embedded fabric, and the principle of measuring joint angles with strain sensors. The sensor in this work employs hook-and-loop fasteners, instead of the embedded fabric from Mengüç et al. (2013), to enable quick, adjustable placement of the sensors (Figure 3A). Furthermore, the sensors in this work were made in three sizes to match the kinematics of the three joints being measured (as detailed in Section 2.3.1). The new sensors also introduce stiffness gradients (Section 2.3.2) achieved, in part, through the introduction of different types of silicone rubber. In total, the four main materials of the sensors in this work were the eutectic gallium indium (eGaIn) alloy as the liquid metal (AlfaAesar, Ward Hill, MA, USA), the two types of silicone rubber as the elastomers (EcoFlex 0030 and SORTA-Clear 40, both from Smooth-On, Easton, PA, USA), the custom printed flexible circuit boards for electrically contacting the liquid metal, and the hook-and-loop fasteners that attach the sensor to the garment base (Loop 3008 type, Velcro USA Inc., Manchester, NH). By introducing these materials and designs, we created reliable electrical and mechanical interfaces from the soft sensors to the rest of the wearable system.

2.3.1. Sensor dimensions. To accommodate body kinematics in the sagittal plane, we made three sizes of sensors with total lengths (which includes the length of elastomer and the hook-and-loop fastener) and extensible lengths (which includes only the length of elastomer) of 155 mm (95 mm extensible), 145 mm (85 mm extensible), and 135 mm (70 mm extensible) to match the expected strains across the hip, knee, and ankle, respectively. The dimensions were found for a 99th percentile male from anthropometric measurements (Henry Dreyfuss Associates, 2002) and confirmed by measuring the range of motion of a male participant of the same size. The cross-sectional geometry of the liquid metal microchannels were identical for all sensors, with a rectangular cross section of 300 μm by 150 μm (Figure 3B). The total sensor elastomer thickness was also identical for all sensors, at 2 mm.

2.3.2. Discretized stiffness gradient. An important design consideration for increased sensor robustness was the use of *discretized stiffness gradients*, which we define as the non-continuous progression in stiffness from a spatial point of view (Figure 3B). Our use of discretized stiffness gradients is inspired by continuous stiffness gradients found in nature, such as squid beaks where there is a two order of magnitude progression in Young's modulus from the stiff beak to the soft body (Miserez et al., 2008). In the case of the soft sensor presented here, there is a six order of magnitude progression of Young's modulus (E) from copper wiring ($E \approx 1.2 \times 10^{11}$ Pa) to the soft elastomer ($E \approx 3.0 \times 10^{4}$ Pa for Ecoflex 0030 (Boonvisut et al., 2013)). To reduce the steepness of this gradient, here we introduce intervening materials in the form of hook-and-loop fastener ($E \approx 4 \times 10^{9}$ Pa for the nylon that hook-and-loop is made from) and a stiff elastomer ($E \approx 1.3 \times 10^{6}$ Pa for SORTA Clear 40 as estimated by its Shore A 40 durometer value and the conversion factor to Young's modulus from Qi et al. (2003)). The discretized stiffness gradient approach reduces the stiffness mismatch between materials from six orders of magnitude (from copper wire to soft elastomer) to at most three orders of magnitude (from hook-and-loop fabric to stiff elastomer).

2.3.3. Principle of sensing. The sensing element is a channel of eGaIn alloy embedded within the elastomer body of the sensor. As the elastomer is stretched, it lengthens in the direction of stretch and contracts transversely according to the material's Poisson ratio. The lengthening and transverse contraction of the elastomer proportionally deforms the channels, which causes an increase in the electrical resistance through the liquid metal path according to the following relationship:

$$\Delta R = \rho \left[\frac{L + \Delta L}{(w + \Delta w)(h + \Delta h)} - \frac{L}{wh} \right] \tag{1}$$

where ΔR is the change in electrical resistance, ρ is the electrical resistivity of the liquid metal (for eGaIn (Dickey et al., 2008), $\rho = 29.4 \times 10^{-8} \Omega \text{ m}^{-1}$), L, w and h are the length, width and height of the channels, and ΔL, Δw and Δh are the changes in length, width and height (Park et al., 2012). For incompressible materials, the Poisson's ratio is $\nu = 0.5$. The relationship between change in length, height, and width of the sensor is defined by the strain, $\epsilon = \Delta L/L$, such that $\Delta w = -\nu\epsilon w$ and $\Delta h = -\nu\epsilon h$. Applying these geometric constraints, the above equation simplifies to

$$\Delta R = \frac{\rho \epsilon L(8 - \epsilon)}{wh(2 - \epsilon)^2} \tag{2}$$

These sensors were implemented as joint angle sensors by correlating their output to changes in the distance between two points connected across a joint (Figure 4). As a first-order approximation, the change in length between these points can be related to the change in the joint angle and scaled by the radius of the joint, that is, $\Delta L = f(\Delta\theta)$, where ΔL is the length change between two points on the body, and hence the strain of the sensor, and $\Delta\theta$ is the change in joint angle. The function, $f()$, transforms the change in joint angle to a change in sensor strain, and in the simplest case we assumed that the given human joint is approximated by a cylindrical rotation with radius r, such that $f(\Delta\theta) = \Delta\theta r$, hence $\Delta L = \Delta\theta r$. Combining this geometric function with the above constitutive equation gives the governing equation of the sensor response to body joint rotation as follows:

$$\Delta R = \frac{\rho L(8 - (\Delta\theta r/L))}{wh(2 - (\Delta\theta r/L))^2} \left(\frac{\Delta\theta r}{L} \right) \tag{3}$$

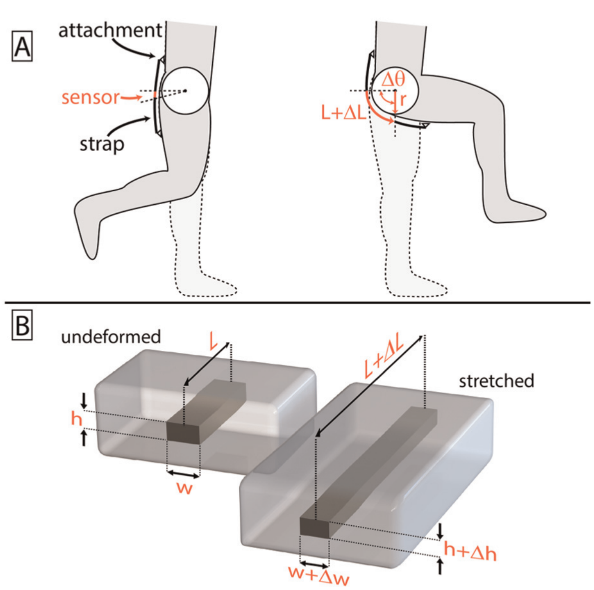

Fig. 4. (A) The change in length between two points on the surface of the body, ΔL, across an approximately cylindrical joint is related to the joint's radius, r, and change in angle, $\Delta\theta$. (B) The resulting deformation of the liquid metal channel is schematically represented by its axial strain lengthening, $L + \Delta L$, and the corresponding transverse strain contraction, $w + \Delta w$ and $h + \Delta h$.

3. Sensor fabrication

The basic process employed to create soft sensors (Park et al., 2010; Majidi et al., 2011; Kramer et al., 2011) was based on the fabrication of microfluidic channels (Whitesides, 2006) as applied to microfluidic electronics (Cheng and Wu, 2012). The fabrication steps include: casting polymers in molds to replicate channel features, laminating layers of the cast polymer to seal the channel features, then filling the channels with liquid metal. In the literature, microfluidic molds are often made through soft lithography (Xia and Whitesides, 1998), but we used 3D printing in our process, which limited feature sizes to a minimum of approximately 100 μm, but enabled rapid design and prototyping of new molds within 24 hours. The molds were printed from a rigid acrylic photopolymer (Objet VeroBlackPlus RGD875 printed on a Connex500, both from Stratasys, Edina, MN, USA). The fabrication approach used in this work built on the fundamental process of casting–laminating–filling established previously.

As was outlined in Section 2.3 above, we introduced materials and designs to create reliable electrical and mechanical interfaces from the soft sensors to the rest of the wearable system. These new materials and designs include the use of hook-and-loop fastener, custom-made flexible printed circuit boards (PCBs), and a discrete gradient of material stiffness. In previous soft sensors electrical wiring proved mechanically fragile because of the large stiffness difference between wires and the embedded flexible PCBs (Mengüç et al., 2013). Here we used the embedded hook-and-loop to our advantage by exploiting the relatively stiff hook-and-loop material (estimated Young's modulus, E $\approx 4 \times 10^9$ Pa) as a strain-relieving material between the flexible PCB and external wiring. To improve the mechanical interface between the embedded hook-and-loop and the soft rubber (E $\approx 3.0 \times 10^4$ Pa for Ecoflex 0030), we added a second, stiffer, silicone rubber (E $\approx 1.3 \times 10^6$ Pa for SORTA Clear 40) that encapsulated the hook-and-loop. Silicone rubber does not create a strong covalent bond to most materials, so we embedded the hook-and-loop fastener such that the loop side was interpenetrated by liquid rubber during the fabrication process (Figure 5C). The full fabrication process is schematically outlined in Figure 5.

4. Experimental methodology

We tested individual sensors in isolation to characterize their robustness and nominal electrical and mechanical behaviors. We also characterized the ability of the sensors to track the sagittal plane leg joint angles of three healthy male participants.

4.1. Characterizing individual sensors

To characterize individual sensors we used three kinds of tests while observing several characteristics. The three tests were (1) extreme extension to failure, (2) moderate

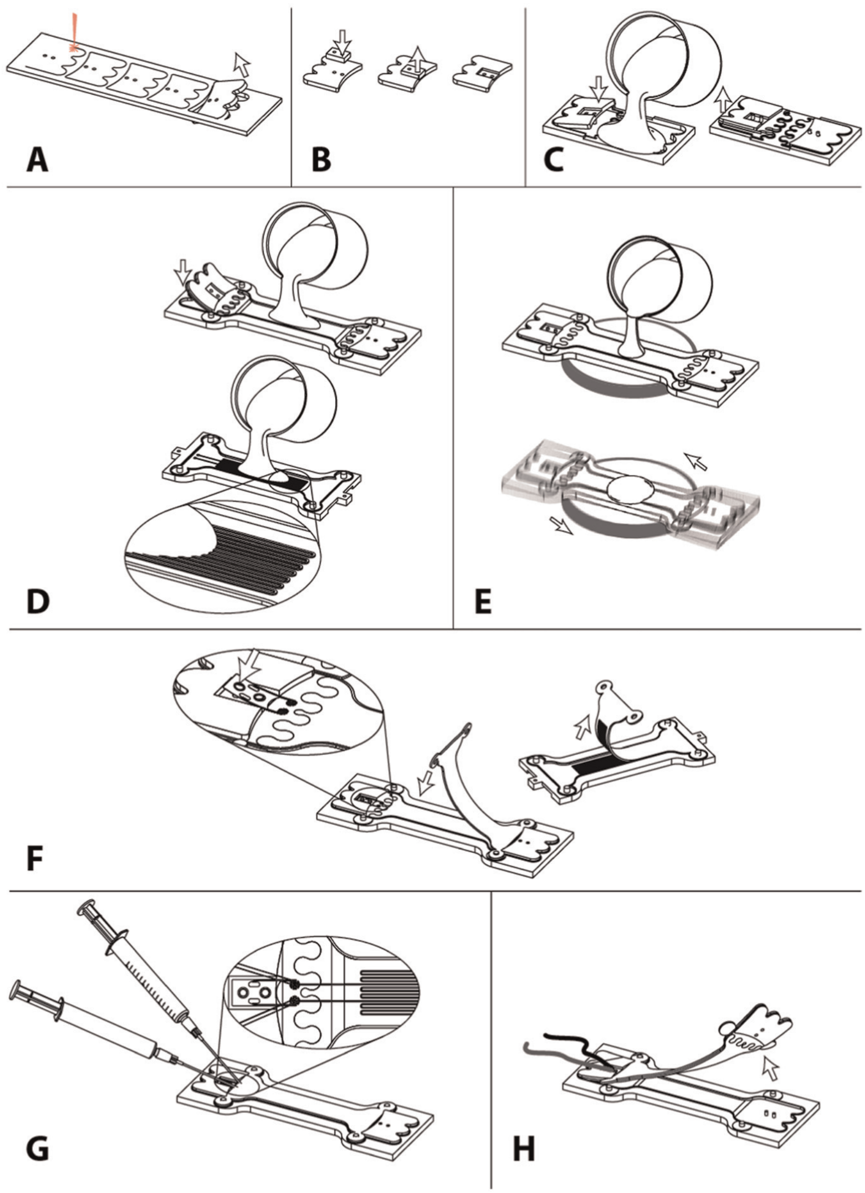

Fig. 5. The soft sensors require the inclusion of several materials and fabrication steps. (A) The hook-and-loop fastener was laser cut into desired shapes. (B) Part of the hooks side of the hook-and-loop was flattened with a stamp heated to 150° C. (C) The hook-and-loop was placed in matching molds and encapsulated in stiff silicone rubber. (D) The encapsulated hook-and-loop was then placed in the bottom-half mold and both it and the top-half mold were cast with soft silicone rubber. (E) After curing the bottom-half mold, a small amount of soft silicone rubber was spun on to it to act as an adhesive layer for lamination. (F) A flexible circuit board was added to the bottom-half sensor, then the top-half sensor was demolded and laminated to the bottom-half. (G) Liquid metal alloy was injected into the microchannels with one needle while a second was used to evacuate the entrapped air. (H) To complete the sensor, wires were soldered to the exposed flexible circuit and encapsulated with rigid epoxy for strain relief.

Table 1. Overview of the three participants' heights and masses, in bold, with general population anthropometry listed for context. The percentiles in the first column are with respect to height.

		Percentile	Height (m)	Mass (kg)
		99	1.92	111.2
Participant	**2**	**85**	**1.83**	**76.6**
	1	**74**	**1.8**	**79.4**
		50	1.755	78.4
	3	**12**	**1.67**	**66**
		1	1.59	45.6

extension for 1500 cycles, and (3) extreme compression to failure. The observed characteristics included force versus strain, electrical resistance versus strain, gauge factor response to cyclic loading, stiffness response to cyclic loading, and sensor failure modes. All isolated tests were conducted on a materials testing machine (model 5544A, Instron Inc., Norwood, MA). The extension rate used, 25 mm/s, was the mechanical limited on the materials testing machine. Although sufficient to get an initial understanding of sensor behavior, we estimate that biomechanically relevant extension rates will be between 120 and 165 mm/s based on a person running at 3 m/s with a step frequency of 3 Hz (Cavagna et al., 1997) and sensor extensions between 40 and 55 mm.

4.1.1. Extension testing. Extension tests were conducted on an isolated sensor with resistance values recorded simultaneously with force and extension values. To determine the strain, the initial length, L, was defined as the extensible portion (i.e. only including the length of elastomer in the sensor, not the additional length of embedded hook-and-loop): 95 mm, 85 mm, and 70 mm for hip, knee, and ankle, respectively. Three ankle sensors were extended to failure to also study the repeatability of sensor robustness.

4.1.2. Cyclical load testing. The reliability of wearable soft sensors was dominated by the mechanical fatigue of the constituent materials. As such, an important test is the cyclic loading of our sensors in extension. One of each size of sensor (ankle, knee, hip) was loaded 1500 cycles to twice the maximum extension expected while on the body. These maximum extensions were experimentally identified for an extreme case by taking measurements on a 21-year-old male colleague who was considered because he represented the 99th percentile in height. The extension (and strain) amounts were 113 mm (119%), 85 mm (100%), and 80 mm (114%), for the hip, knee, and ankle sensors, respectively. The maximum extension rate possible on the materials tester, 25 mm/s, was used for all three sensor types.

4.1.3. Compression testing. Our sensor placement onto the body specifically avoided bony landmarks to reduce sensitivity to pressure or impacts on the body. From previous work we had seen that the sensor will change electrical resistance in both axial extension and transversal compression (Park et al., 2012). To have a better understanding of the sensors' limits under extreme compressive loads, such as falls and impacts, we compressed a single sensor to failure with a 10 mm diameter plastic flat punch using the Instron materials tester. The center of the sensor was indented gradually at a rate of 0.0167 mm/s while its electrical resistance was recorded. The flat punch size was chosen to match previous studies (Park et al., 2012; Vogt et al., 2013), but the indentation rate chosen was much slower to reduce rate-dependent viscoelastic effects.

4.2. Characterizing soft sensors for tracking body motion

Three healthy males under the age of 30 were recruited as participants (heights and masses are reported in Table 1). The three participants gave written, informed consent before inclusion in the study. None of the participants had physical impairments that would have affected their gait during the experimental protocol. The Harvard Medical School Committee on Human Studies approved the protocol. All human motion studies took place in the Wyss Institute Motion Capture Laboratory. During motion capture we focused on one task: locomotion by the participant at predefined speeds on an instrumented split-belt treadmill (Bertec Corporation, Columbus, OH). Each participant performed three 60-second trials at each of five speeds (0.89, 1.3, 1.8, 2.2, and 2.7 m/s), resulting in just over 5000 recorded steps in total. The participants' kinematics were collected with optical motion capture using 39 passive retro-reflecting markers and eight infrared cameras (Vicon T40S, Oxford Metrics, Oxford, UK). Signals from the sensor suit were synchronized with the Vicon system's through a direct cable connection that gave a 5 V analog signal for the duration of data collection. The sensor signals were collected as 8-bit digital values from the microcontroller (Figure 2) then post-processed by linearly fitting to the body angles determined from the optical motion capture inverse kinematics detailed below.

The optical motion capture system was calibrated using the standard passive Vicon calibration wand, with the Vicon Nexus software automatically calculating the calibration matrix. The spatial resolution of the system depended heavily on the marker size, separation, and distance from cameras. For our system setup, each camera sensor had 4 megapixel resolution, the marker diameter was 9.5 mm, the average distance between markers and camera was 4 m, and the field of view was $67° \times 52°$, which allows us to calculate a pixel size of 2.2 mm/pixel. The mean image error reported by Vicon Nexus for our eight camera system was less than 0.2 pixels; the image error represents the system level accuracy based on the combined reconstruction from all cameras. As such, we can estimate an absolute static spatial accuracy of 0.44 mm for our system.

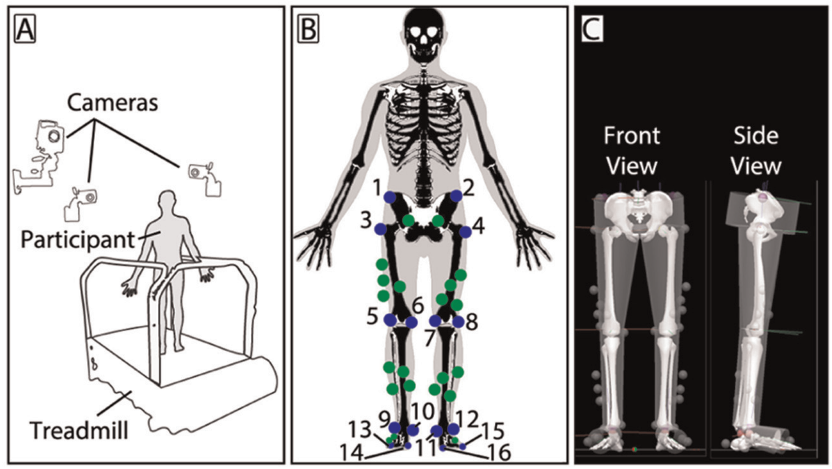

Fig. 6. (A) Schematic representation of the experimental setup, with the participant on the treadmill and cameras positioned on the walls. (B) Optical motion capture markers were placed at tracking locations (green circles) and the following anatomical locations (blue circles): 1, right apex of iliac crest; 2, left apex of iliac crest; 3, right greater trochanter; 4, left greater trochanter; 5, right lateral femoral condyle; 6, right medial femoral condyle; 7, left medial femoral condyle; 8, left lateral femoral condyle; 9, right lateral malleolus; 10, right medial malleolus; 11, left medial malleolus; 12, left lateral malleolus; 13, superior aspect of the right fifth metatarsophalangeal joint; 14, superior aspect of the right first metatarsophalangeal joints; 15, superior aspect of the left first metatarsophalangeal joint; 16, superior aspect of the left fifth metatarsophalangeal joint. (C) The resulting kinematic reconstruction used for calculating the joint angles from optical motion capture.

The 39 passive, retro-reflecting markers were positioned on participants according to a modified Cleveland Clinic marker set (Figure 6A). The Cleveland Clinic marker set is a ‘cluster-based’ marker set, in which clusters or arrays of three markers are used to define joint centers and segmental coordinate systems. We modified the Cleveland Clinic set by using clusters of four markers instead of clusters of three markers, to improve the ability to detect at least three markers in case of obstruction (Cappozzo et al., 1997). The marker placement was guided by performing manual palpations over bony landmarks, which is a standardized procedure to achieve better measurement reproducibility, data comparison, and data exchange (van Sint Jan, 2007). Quad marker clusters (seen as green circles in Figure 6A) were placed on the thighs and shanks. The human static pose calibration was based on established techniques (Kadaba et al., 1990; Winter, 1990), whereby each participant took a relaxed bipedal standing pose with two arms stretched out, at which point a static trial of four seconds was conducted and the subtalar joint positioned in neutral (0°) by the examiner in the motion capture lab. Motion capture data was collected at a sampling rate of 120 Hz.

Visual 3D v4 (C-Motion, Germantown, MD, USA) was used to build a 7-segment model with 18 degrees of freedom (Figure 6B). Inverse kinematics were performed to calculate anatomical joint angles given the three-dimensional marker trajectories. In Visual3D the inverse kinematics problem was solved as a global optimization problem, which computes the pose of a model that best matches the optical motion capture data in terms of a global criterion. The initial solutions to this problem were based on (Lu and O’Connor, 1999). Soft tissue artifacts will affect the 3D coordinates of the markers and thus the reconstructed joint angles that were used to compare and fit our sensors. Such artifacts are a known source of variability in on-the-skin sensors, but we accounted for it by our comparison of the precision of the soft sensors to that of optical motion capture (Table 3). In future work it may be possible to compensate for soft-tissue artifacts with automated algorithms (Gabiccini et al., 2013).

5. Results and discussion

Here we present results of testing individual sensors in isolation to characterize their robustness and nominal electrical and mechanical behaviors. In addition, we present results of characterizing the sensor suit’s ability to track the sagittal plane leg joint angles of three healthy male participants. We discuss the meanings of the results throughout, and present a discussion on the sources of error for soft wearable sensing.

5.1. Individual sensor results

We characterized the individual sensors for their nominal behavior in several ways, including the mechanical and electrical behavior under uniaxial strain and cyclic stretching, the ultimate strain required to break the sensors, and the response of the sensors to compressive loading. Through these assessments we quantified the electrical and mechanical specifications of the sensors, and prove their overall robustness. The results of our characterization of the sensors are summarized in Table 2.

Table 2. Summary of sensor characterization results.

Sensor	Electrical Gauge factor	Hysteresis (%)	Linearity	Gauge change (%/1500 cycles)
Hip	2.5	7.8	0.77	0.50
Knee	2.4	3.9	0.91	0.05
Ankle	2.2	4.3	0.92	2.00

Sensor	Mechanical Stiffness (N/m)	Hysteresis (%)	Linearity	Stiffness change (%/1500 cycles)	Max extension (mm)
Hip	17	10.5	0.91	2.5	235
Knee	21	7.0	0.95	0.34	274
Ankle	33	10.8	1.09	1.4	277

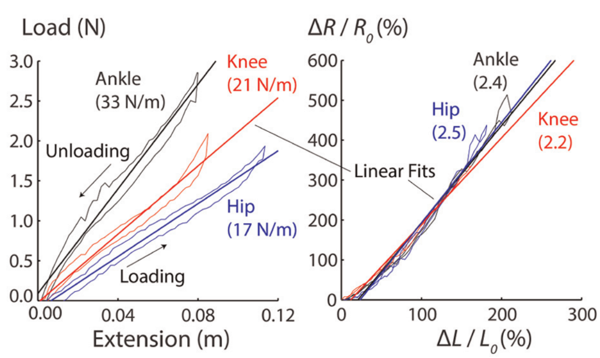

Fig. 7. (Left) The load versus extension characterization revealed the ankle sensor as the stiffest and the hip sensor as the most compliant. (Right) The sensor's change in electrical resistance was compared with change in length to reveal highly linear behavior and similar gauge factors for the different sizes.

5.1.1. Results of extension testing. The mechanical loading and unloading of the three sensor types revealed overall linear behavior with some hysteresis (Figure 7, left plot). Hysteresis was calculated as the maximum difference between the loading and unloading traces as a percentage of the maximum load value. Linearity was calculated as the ratio of the area under the curve of the loading trace to the area of a triangle formed by the origin point, the maximum strain point, and the maximum load point. The sensors had mechanical hysteresis percentages (and linearity ratios) of 10.5% (0.91 linearity), 7.0% (0.95), and 10.8% (1.09) for the hip, knee, and ankle, respectively. The hysteresis and linearity of the elastomer sensors are consistent with the expected behavior of viscoelastic materials (Meyers and Chawla, 2008).

Our characterization of the three sensor types under extension also revealed that all three had different axial stiffnesses (Figure 7, left plot). The stiffness of each sensor is based on its geometry: all have the same thickness, T = 2 mm, and width, W = 15 mm, but differing extensible lengths of L_{ankle} = 70 mm, L_{knee} = 85 mm, and L_{hip} = 95 mm. The elastomer used to make the sensors has a reported modulus, E, from 30 to 100 kPa. If we considered the sensors to be ideal springs, then by Hooke's law, $k = (EWT)/L$, we would expect the spring stiffnesses to be k_{hip} = 9.5 to 32 N/m, k_{knee} = 11 to 35 N/m, and k_{ankle} = 13 to 43 N/m. The observed stiffness values were 17, 21, and 33 N/m for the hip, knee, and ankle sensors, respectively. The observed deviations from theoretical values might be attributed to the geometric differences in the actual shape of the sensor and inclusion of liquid metal channels.

It was also relevant to compare the maximum forces of the sensors with the expected joint torques of the user to identify possible impact on normal gait kinematics. As an example, for a 99th percentile male we would expect a weight of 111.2 kg and joint radii of 0.094, 0.064, and 0.051 m for the hip, knee, and ankle, respectively (Henry Dreyfuss Associates, 2002). The maximum forces exerted by the sensors for a normal range of motion was experimentally observed from extension tests to be 1.8, 2, and 2.9 N for the hip, knee, and ankle, respectively (see Figure 7). From the literature, we found that maximum joint torques normalized to body weight during normal walking on level ground were reported as 1, 1, and 2 Nm/kg for the hip, knee, and ankle, respectively (Winter, 1984). Assuming the sensors apply their force at a moment-arm equal to the joint radius, then the expected torques applied by the sensors (and percent of actual joint torques) would be 0.17 (0.17%), 0.13 (0.13%), and 0.15 Nm (0.075%) for the hip, knee, and ankle, respectively. Under these assumptions, the sensors would exert less than one fifth of one percent of max joint torques, which is indicative of the minimal impact they would have on natural gait kinematics of the wearer.

In the normalized signal of the sensors in response to strain (Figure 7, right plot), one can see that the sensors had very low hysteresis and reasonable linearity. The

Table 3. Sensor variability comparison: values reported are standard deviations in degrees. The Mann–Whitney *U*-test results indicated no statistically significant difference between the soft sensor and optical motion capture standard deviations under analysis at the 5% significance level.

				Locomotion speed (m/s)				
		Joints	Sensor	0.89	1.34	1.79	2.24	2.68
Participant	1	**Hips**	Soft	1.2	1.1	1.2	1.5	1.6
			Optical	*1.2*	*0.9*	*1.1*	*1.3*	*1.4*
		Knees	Soft	2.2	2.0	1.9	2.9	3.0
			Optical	*2.4*	*2.0*	*2.0*	*2.5*	*2.9*
		Ankles	Soft	1.2	1.0	0.9	1.8	1.9
			Optical	*1.7*	*1.4*	*1.6*	*2.3*	*2.4*
	2	**Hips**	Soft	1.7	1.3	1.4	2.0	2.6
			Optical	*1.3*	*1.1*	*1.2*	*1.6*	*1.7*
		Knees	Soft	3.2	2.3	2.3	3.4	4.7
			Optical	*2.2*	*2.0*	*2.0*	*2.6*	*2.8*
		Ankles	Soft	1.6	1.4	1.6	2.2	2.6
			Optical	*1.7*	*1.5*	*1.5*	*2.2*	*2.4*
	3	**Hips**	Soft	1.2	1.2	1.7	1.7	2.0
			Optical	*1.1*	*1.0*	*1.5*	*1.3*	*1.6*
		Knees	Soft	2.0	2.1	2.4	3.0	3.2
			Optical	*2.0*	*1.9*	*2.3*	*2.5*	*2.9*
		Ankles	Soft	1.0	1.0	1.5	2.4	2.4
			Optical	*1.4*	*1.3*	*2.0*	*2.1*	*2.2*
Mean		**All**	Soft	1.7	1.5	1.7	2.3	2.7
			Optical	*1.7*	*1.5*	*1.7*	*2.1*	*2.2*
		U-test *p*-values		0.951	0.388	0.746	0.076	0.661

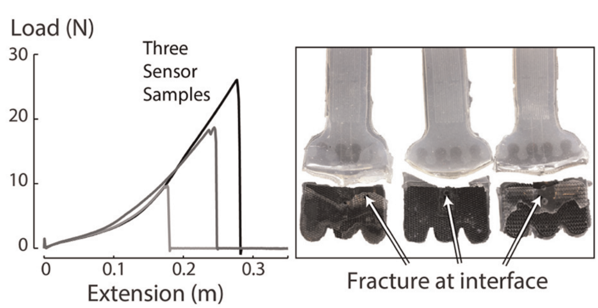

Fig. 8. (Left) Results of extending three sensor samples of the same type (ankle sensors) revealed different strengths at failure due to manufacturing variability. (Right) In all three cases the failure occurred at the interface between the stiff silicone rubber ($E \approx 1.3$ MPa) and hook-and-loop fastener (made of nylon, $E \approx$ 4 GPa).

sensor signals had electrical hysteresis percentages (and linearity ratios) of 7.8% (0.77 linearity), 3.9% (0.91), and 4.3% (0.92) for the hip, knee, and ankle, respectively. The linearity of the electrical response was because the sensor resistance is directly related to geometric effects, and so is insensitive to the stiffness of the material. A linear fit to the signal was used to calculate gauge factors of 2.5, 2.4, 2.2 for the hip, ankle, and knee sensors, respectively (Figure 7). These observed gauge factors under uniaxial strain are similar to our previous liquid-metal embedded elastomer sensors where we found 3.1 for Mengüç et al. (2013) and 3.6 for Park et al. (2012).

The soft sensors were manufactured by hand and as such there was some variability in their behavior. The mechanical behavior was very consistent for extensions less than 200%, as can be seen from results of individual sensors under moderate load (Fig 7), but the variability became more significant when sensors were extended to failure (Figure 8). When three sensors of the same type (ankle sensors) where stretched excessively, they failed at extensions of 173, 237, and 277 mm, which correspond to strains of 247%, 339%, and 396%, respectively. Although there was variability in sensor failure length, the expected amount of extension on the ankle of a wearer was much less, on the order of 80 mm corresponding to a strain of 114%, which gave our ankle sensor a minimum factor of safety of 2.2.

In the case of the hip and knee, the extension (and strain%) amounts had been experimentally identified as 113 mm (119%) and 85 mm (100%), respectively. A single hip sensor was stretched to a failure point of 235 mm (247% strain, factor of safety 2.1) and a single knee sensor was stretched to 274 mm (322% strain, factor of safety 3.2). The hip and knee sensors were also more than robust enough for the expected ranges of motion.

It should also be noted that though the sensors failed at different amounts of extension, the failure mode was very similar and the fracture location was consistently at the interface of the stiff silicone rubber ($E \approx 1.3$ MPa) and the hook-and-loop (made of nylon, $E \approx$ 4 GPa). The failure mode showed a clear weak point of the sensor where there is a difference of three orders of magnitude in Young's modulus between materials. The material stiffness mismatch

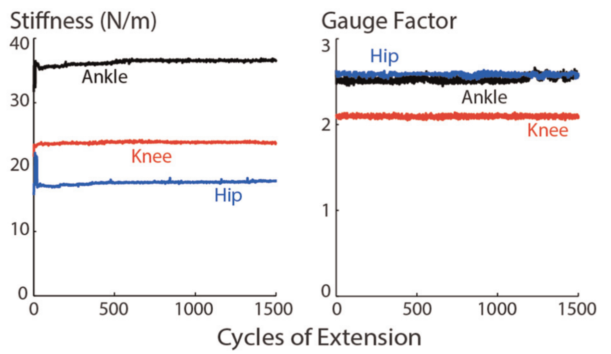

Fig. 9. The sensors were mechanically and electrically consistent for over a thousand cycles of extension. The extension (and strain) amounts were 80 mm (215%), 85 mm (161%), and 113 mm (181%) for the ankle, knee, and hip sensors, respectively. The extension rate was 25 mm/s for all three sensor types.

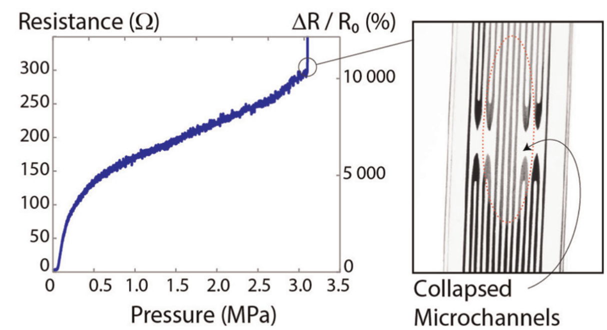

Fig. 10. The results of compressing the center of a sensor with a 10 mm diameter flat-punch revealed the nonlinear electrical response of the sensor as well as its mechanical robustness. The back-lit photograph on the right showed the region that was compressed during the experiment and revealed the collapsed microchannels as a much lighter shade of gray in comparison to the non-collapsed microchannels which were nearly opaque. After collapsing, the microchannels could be healed by massaging them.

can be reduced in future designs by including greater number of steps in our discretized stiffness gradient.

5.1.2. Cyclic loading results. Similar to the consistency of the gauge factor during the cyclic tests, the stiffness of the sensors was also stable through repeated loading (Figure 9, left plot). Changes in stiffness were calculated as the slope of a linear fitting over the duration of the entire experiment which captures the overall behavior and rejects initial variability in measured values. Over the course of 1500 cycles of extension the ankle sensor increased in stiffness by 1.4%, the knee sensor stiffness increased by 0.34%, and the hip sensor stiffness increased by 2.5%.

The gauge factor of the sensors showed excellent consistency over the duration of 1500 cycles of extension (Figure 9, right plot). As in stiffness change calculations, changes in gauge factor were calculated from a linear fitting over entire data set. The ankle sensor gauge factor changed by 2% during the entirety of the test, the hip sensor gauge factor changed by 0.5%, and the knee sensor changed by less than 0.05%.

5.1.3. Compression results. A potential complication in the use of liquid metal embedded elastomer sensors was the cross-sensitivity to compression (Figure 10). In characterizing the sensitivity to pressure, we found that at 3 MPa of pressure (236 N applied with a 10 mm diameter cylinder), the electrical path was cut due to microchannel collapse. This pressure was equivalent to placing a mass of 24 kg on the contact area of an index finger tip (≈10 mm diameter) or a mass of 385 kg on the contact area of patella (≈40 mm diameter). A post-experiment close-up view of the sensor (top right inset in Figure 10) showed how the microchannels were collapsed and devoid of liquid metal alloy. However, this failure mode was not permanent, and the sensor was fixed by manually massaging the microchannels to restore the spacing in the microchannels. This observed characteristic was important for the sensor's overall usability, and future work will explore means to mitigate compression-induced failure or provide information to users on how to restore function after inadvertent overloading.

5.2 Results of tracking body motion with soft sensors

We characterized the effectiveness of the sensors for wearable applications in two ways: the precision of the sensor signal (expressed as the standard deviation and compared with the standard deviation of optical motion capture), and the accuracy of the sensors (expressed as the root mean square (RMS) error in comparison to optical motion capture). In addition to these quantitative assessments we also present a discussion on the sensors' merits for use in soft wearable robotic systems.

The linear fitting (Figure 11) of sensor signals to joint angles determined from optical motion capture was done for the entire length of time of each trial for each participant. In this way the linear fitting was not treated as or validated as a calibration procedure. However, future work must include the validation of sensor calibration for trials in the field and the development of calibration that does not use any external optical motion capture. One potential approach is to initially perform a single calibration for a specific user in a lab setting to set a baseline of expected kinematics and ranges of motion, then recalibrate each time the same user doffs and dons the sensors. Calibration could be accomplished with a rich set of information, such that there is enough information content in the motion to determine the sensor's placement, similar to system identification or model identification approaches. Alternatively, a

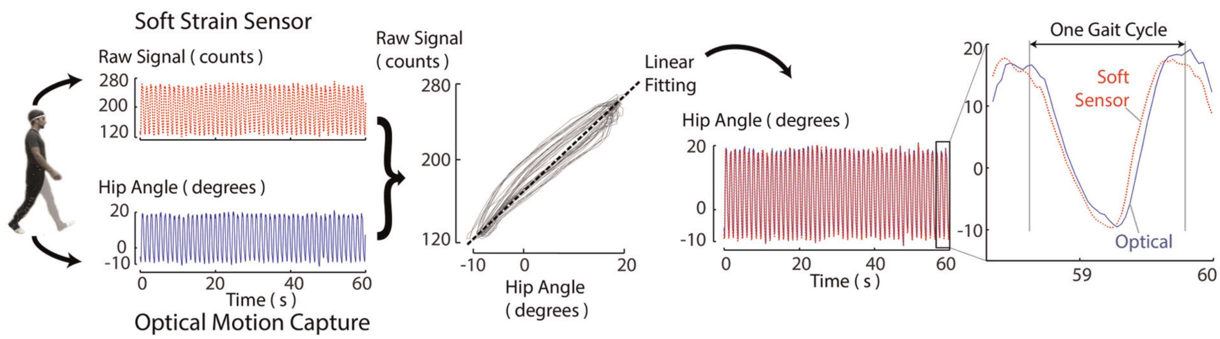

Fig. 11. The soft strain sensors were calibrated with anatomical joint angle information processed from optical motion analysis. From left to right: the raw digital signals from the sensors (in counts) were collected synchronously with the joint angle (the right hip in this case). The raw sensor signal from the entire 60 second trial was fitted to the joint angle to calibrate the sensor.

simple set of information could calibrate the sensors to specifically performed actions in a manner that is similar to its usage goals in the field, e.g. take 10 steps to calibrate the sensors for level-ground walking.

As was observed in isolated sensor tests where the sensor characteristics were consistent for over a thousand cycles, the sensors also exhibited consistent performance when worn on the body. This can be observed in the results of the soft sensors compared with optical motion capture, where the six anatomical joints of a single participant (number 3) were analyzed at three speeds. A subset of the total trials are presented in Figure 12 to serve as a visual example of the sensor behavior. Each shaded line in Figure 12 is centered at the mean, with the width indicating one standard deviation about the mean (i.e. a thicker line indicates greater variability in the signal). These data shows that the sensors had low variability in their signals, and we found the average standard deviation across all participants to range from 1.7° for walking up to 2.7° for running (Table 3). It is important to note that the variability of the sensor measurements was confounded by the participant's natural variability. As a comparison, we calculated that the optical motion capture gave average standard deviations across all participants from 1.7° for walking up to 2.2° for running. After confirming normality of the data through Lillefor's test and rejecting homogeneity of variance through Levene's test, we tested for statistical difference between the soft sensor and optical motion standard deviations using the non-parametric Mann–Whitney *U*-test. The results of the *U*-test indicated that there was no statistical difference between the soft and optical standard deviations under a 5% significance analysis (Table 3, bottom row). Future work will address this confounding factor by characterizing the sensors on an anthropomorphically correct robotic leg model to control for variability. Even so, we see similar degrees of variability in the soft sensors and the optical motion capture.

From the evaluation comparing soft sensors with optical motion capture, it is clear that the sensors can record the actual joint angles more accurately at slower speeds when the participant is walking compared to running at higher

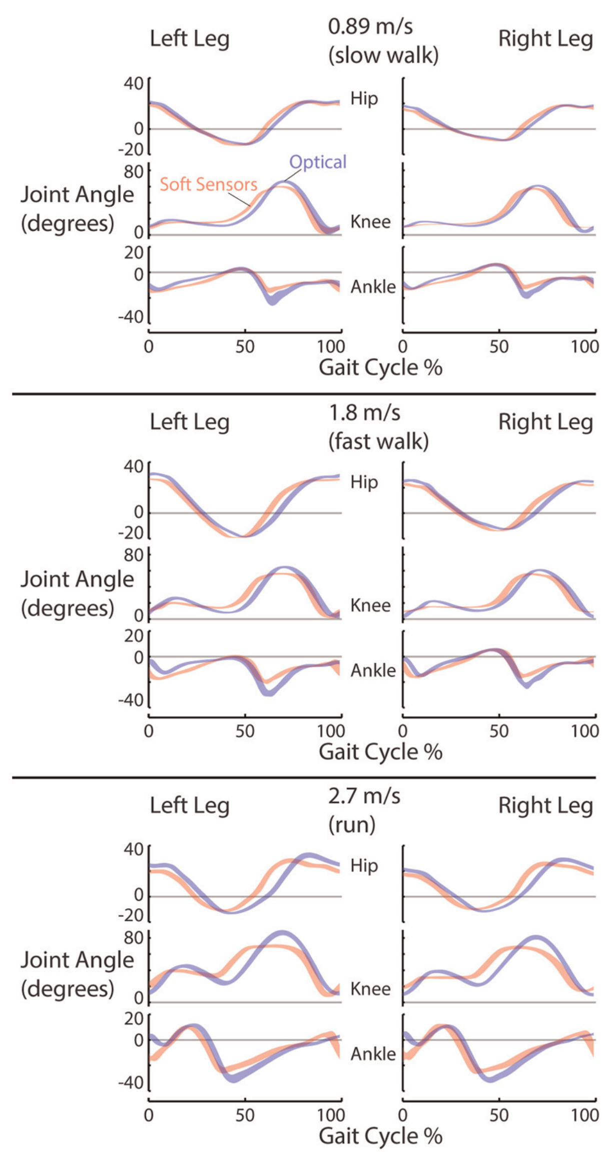

Fig. 12. The angles of all six lower limb joints as tracked by the soft sensors (in red) and optical motion capture (in blue). Each shaded line is centered at the mean, with the width indicating one standard deviation about the mean; a thicker line indicates greater variability in the signal. Note the gait pattern change in joint angles between walking (1.8 m/s) and running (2.7 m/s).

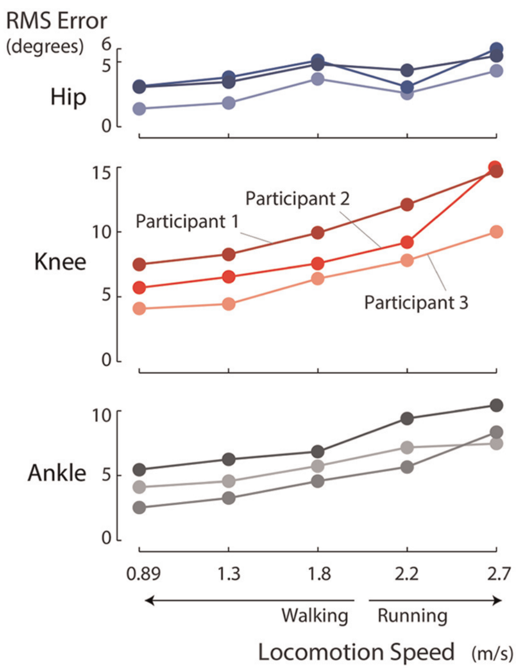

Fig. 13. Taking the optical motion capture system as the true signal, the sensor response was evaluated for its RMS error. All signal data from each sensor on each participant during a total of three trials at each speed is represented here. The individual participants had slightly varying magnitudes of error, but all sensors showed increasing error with increasing locomotion speed of the individual.

speeds (Figure 13). At the worst case, the maximum RMS error was nearly 15° for the knee sensors on participants 1 and 2 when running at 2.7 m/s. Despite the drop in accuracy, we found that the soft sensors' signals were as precise as the optical motion capture, i.e. the sensor had the same variability for the same gait pattern. Interestingly, the error of the hip sensors decreased slightly between fast walking and running due to the decrease in hip motion after the change in gait.

Observations of the participants while walking and running revealed that the sensors have particular dynamics as a result of rate-dependent viscoelastic effects. The linear-fitting of the sensor signal to optical motion capture does not account for the nonlinearity and hysteresis of the sensor, nor does it account for the natural variability in gait. These effects lead to reductions in accuracy, particularly with increased locomotion speeds. Judging from the kinematic recreation in Figure 14, the sensors also have a certain amount of phase lead versus the optical motion capture. It appears that there is a maximum phase lead of approximately 10–15° for each sensor, but at slightly different parts of the gait cycle (between 45% and 65% for the knee, and between 60% and 75% for both the hip and ankle). It is likely that the sensor signals appear to lead the actual joint angles because of limitations in our linear fitting approach. Specifically, we fitted the sensors by applying a linear fit of the sensor data to that from the optical motion capture system in the time domain (Figure 11). This fitting does not consider the changing dynamics of the sensor itself with increasing extension rates. Future work will seek to improve fitting by characterizing and modeling the changing behavior of the sensors as related to extension rate and by applying fits to the signals in the frequency domain.

5.3. Sources of error for soft wearable sensing

This overall behavior of the soft wearable sensors is of poor accuracy but good precision. We must address the sources of error to indicate limitations, potential uses, and future efforts to optimize the soft sensing suit. Possible approaches to improving accuracy include improving garment integration by increasing stiffness of the sensors or direct bonding of sensors fully onto garments along their entire length (which would be different from Mengüç et al. (2013) and this work, where the sensors were only attached at their ends). Some error may be coming from the garment base sliding on the skin, however, one simple solution could be to add thin non-slippery pads inside of the tights at the sensor attachment location along with simple straps that tighten the sensor attachments to the skin. Even without problems of slip, any skin-mounted sensor will suffer from soft-tissue artifacts, which must be solved with compensation algorithms (Gabiccini et al., 2013).

A possible source of error is the nonlinearity of the soft sensor response under compression. One of our efforts in this work was to avoid the compression of the sensors by moving their locations from directly on top of joints and bony landmarks to more soft and flat areas of the body. Although this does not completely solve the problem, it reduced the possibility of unnecessary compression events. A possible future effort is adding pressure-sensing elements on top of the strain-sensing element in each sensor, so that each sensor itself has the capability to detect compression in addition to strain (Park et al., 2012; Vogt et al., 2013).

A more optimal (Bianchi et al., 2013a) or redundant placement on the body may improve measurement of the body's natural degrees of freedom. Alternatively, by better characterizing the sensor's relationship between hysteresis and strain rate, it may be possible to compensate for the observed deviation with increasing velocity. Currently, the low variability of the sensor signal is apparent in its small standard deviations (Table 3), but presenting this data in visual models derived by forward kinematics also reveals large instantaneous errors in joint angles (up to 20° on the knee) that make absolute position measurements difficult (Figure 14). As covered above, such observed errors likely emerge from unaccounted slippage, deformation, or other mechanics of soft materials. Accounting for such soft mechanics might be achieved through methods that have embedded models or constraints of body kinematics, such as Kalman filters or particle filters. To develop such model-based filters, we will have to identify the mechanics of soft tissues as well as the interaction of

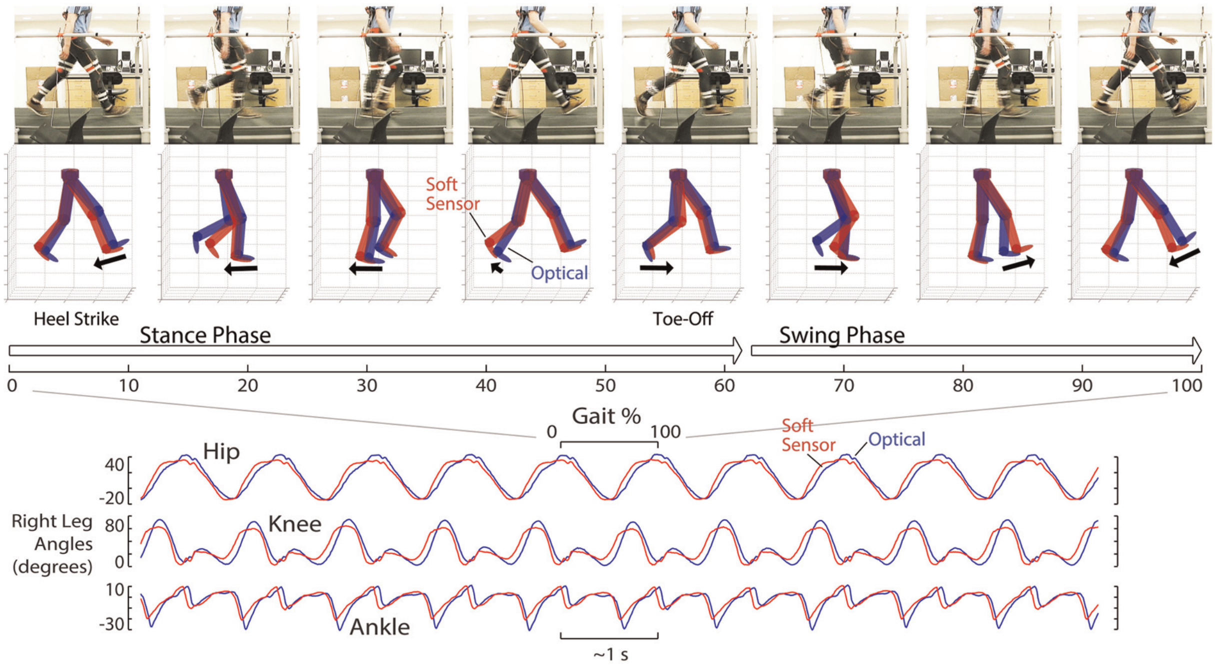

Fig. 14. A small sample of data from participant 2 walking at 1.8 m/s. Still images from the experiment are presented at the top with the anatomical kinematic model recreated for each instance in frames below it. The entire sequence of images is taken from a single gait cycle and shows how qualitatively similar the soft sensor signal is to optical motion capture.

the worn garments with the wearer. Even so, without additional modeling, the sensor signals still provide sufficient gross motion measurement capability that could be useful in understanding the general state and behavior of the wearer. In this way, the sensory information could be used in pattern tracking to identify between walking and running gaits or other pre-trained states, such as stair-climbing, squatting, etc.

6. Conclusions

Soft wearable robots require the development of soft-material technologies analogous to rigid actuators and sensors currently available for traditional robotic systems. The development of such soft devices requires new approaches to design and fabrication in addition to bench top and human subjects experiments to quantify and document their performance. In this paper we presented soft strain sensors and their integration into a soft wearable garment for measuring human hip, knee, and ankle joint angles in the sagittal plane. The development of soft sensing technology requires careful consideration of the interface between them and inextensible components such as electronics, fabrics, and host garments.

Expanding on our previous liquid metal in elastomer sensors (Mengüç et al., 2013; Park et al., 2012), in this work we presented a discretized stiffness gradient design that addresses the imperative need for a mechanical interface between low and high Young's modulus materials. Our interface design highlighted the need for a systematic study of interface mechanics for soft materials similar to what exists for metals and ceramics (Messler, 2004). Even so, the soft strain sensors presented here are the only ones in the literature, to the authors' knowledge, that are sufficiently robust to withstand thousands of repeated loading cycles to hundreds of percent strain and be useful in an integrated wearable suit.

This work also introduces extensive characterization of a wearable soft sensing suit, expanding on our previous work (Mengüç et al., 2013) by now instrumenting both legs, including multiple participants, and increasing the speeds of locomotion. In terms of performance, the nonlinearity and hysteresis of these hyper-elastic sensors and their mechanical interface to a host garment affects the accuracy (although not precision) that can be obtained when making joint angle measurements. We found that sensor readings varied depending on the specific operating condition that affected the strain and strain rate experienced by the sensor. With regards to motion tracking, we found the sensors to be reliable both mechanically and electrically, but that their measured joint angle would deviate with increasing locomotion speed. Importantly, the sensor variability remained low, even when the participant was running. The difficulty of maintaining accurate measures of joint angles, but relative stability of the sensor signal, suggests that it would be more useful for higher-level control (e.g. a state machine to detect walking versus running) as opposed to direct control over the absolute position of the joints. It is also possible that the soft sensors may serve an important role for sensor fusion of different sensors on wearable robot applications. The high spatial and temporal resolution of IMUs may eventually complement the physically compliant and drift-resistant soft sensors to create a new human sensing system.

Future work is required on the anatomical, mechanical, biocompatible, and computational aspects of our soft sensor to improve its reliability and breadth of applications. Anatomically, it will be important to consider the relationship of sensing to anthropometry by performing in-depth analysis of individuals' limb dimensions as well as including both genders. Mechanically, protecting the sensors from inadvertent and/or redundant sensing will enable robust measurements in field settings. Biocompatibility can be improved through the use of ionic liquids as an alternative to liquid metal, which may also enable applications within the body. Computationally, we plan to explore other uses for the rich information that the sensors provide. Pattern recognition, machine learning, and morphological computation may make better use of the sensor signals and are more sophisticated than our off-line linear fitting approach that we have thus far used. Ultimately, a robust calibration procedure must be established to realize the potential for using soft sensors as a new motion capture system.

With further refinement of the system presented here, we can imagine single-piece garments with integrated sensors that can be worn under normal clothing. Such instrumented garments could capture the motion of the wearer's body throughout the day in a low profile and unobtrusive manner. Collecting such a rich set of data could be useful for doctors monitoring an elderly person's daily motion as a means of predicting and preventing the onset of gait pathology or it could be used by professional trainers as a means to assess the motions of athletes during training and recovery. In addition, instrumented garments could be a part of future soft wearable robots that assist the wearer during locomotion or other activities.

Supplementary Materials

Supplementary materials will be provided upon request from the corresponding author.

Funding

This material is based upon work supported by the Defense Advanced Research Projects Agency (DARPA), Warrior Web Program (Contract No. W911QX-12-C-0084). The views and conclusions contained in this document are those of the authors and should not be interpreted as representing the official policies, either expressly or implied, of DARPA or the U.S. Government.

References

Asbeck AT, Dyer RJ, Larusson AF and Walsh CJ (2013) Biologically-inspired soft exosuit. In: *IEEE international conference on rehabilitation robotics*, pp. 1–8.

Bar-cohen Y (2004) *Electroactive Polymer (EAP) Actuators as Artificial Muscles: Reality, Potential, and Challenges*. Bellingham, WA: SPIE.

Bianchi M, Salaris P and Bicchi A (2013a) Synergy-based hand pose sensing: Optimal glove design. *The International Journal of Robotics Research* 32(4): 407–424.

Bianchi M, Salaris P and Bicchi A (2013b) Synergy-based hand pose sensing: Reconstruction enhancement. *The International Journal of Robotics Research* 32(4): 396–406.

Boonvisut P, Jackson R and Cavusoglu MC (2013) Estimation of soft tissue mechanical parameters from robotic manipulation data. *IEEE/ASME Transactions on Mechatronics* 18(5): 1602–1611.

Cappozzo A, Cappello A, Della Croce U and Pensalfini F (1997) Surface-marker cluster design criteria for 3-D bone movement reconstruction. *IEEE Transactions on Bio-Medical Engineering* 44(12): 1165–1174.

Cavagna GA, Mantovani M, Willems PA and Musch G (1997) The resonant step frequency in human running. *Pflügers Archiv* 434(6): 678–684.

Cavallo F, Esposito D, Rovini E, et al. (2013) Preliminary evaluation of SensHand V1 in assessing motor skills performance in Parkinson disease. In: *IEEE international conference on rehabilitation robotics*, pp. 1–6.

Cheng S and Wu Z (2012) Microfluidic electronics. *Lab on a Chip* 12(16): 2782–2791.

Chossat JB, Park YL, Wood RJ and Duchaine V (2013) A soft strain sensor based on ionic and metal liquids. *IEEE Sensors Journal* 13(9): 3405–3414.

Corke P, Lobo J and Dias J (2007) An introduction to inertial and visual sensing. *The International Journal of Robotics Research* 26(6): 519–535.

De Rossi D and Veltink P (2010) Wearable technology for biomechanics: e-textile or micromechanical sensors? *IEEE Engineering in Medicine and Biology Magazine* 29(3): 37–43.

Dickey MD, Chiechi RC, Larsen RJ, Weiss EA, Weitz DA and Whitesides GM (2008) Eutectic gallium-indium (EGaIn): a liquid metal alloy for the formation of stable structures in microchannels at room temperature. *Advanced Functional Materials* 18(7): 1097–1104.

Gabiccini M, Stillfried G, Marino H and Bianchi M (2013) A data-driven kinematic model of the human hand with soft-tissue artifact compensation mechanism for grasp synergy analysis. In: *IEEE/RSJ international conference on intelligent robots and systems*. pp. 3738–3745.

Galiana I, Hammond FL, Howe RD and Popovic MB (2012) Wearable soft robotic device for post-stroke shoulder rehabilitation: Identifying misalignments. In: *IEEE/RSJ international conference on intelligent robots and systems*, pp. 317–322.

Giansanti D, Macellari V, Maccioni G and Cappozzo A (2003) Is it feasible to reconstruct body segment 3-D position and orientation using accelerometric data? *IEEE Transactions on Bio-Medical Engineering* 50(4): 476–483.

Goldfield EC, Park YL, Chen BR, et al. (2012) Bio-inspired design of soft robotic assistive devices: the interface of physics, biology, and behavior. *Ecological Psychology* 24(4): 300–327.

Guizzo E and Goldstein H (2005) The rise of the body bots. *IEEE Spectrum* 42(10): 50–56.

Henry Dreyfuss Associates (2002) *The Measure of Man and Woman: Revised Edition*. New York: John Wiley & Sons.

Kadaba MP, Ramakrishnan HK and Wootten ME (1990) Measurement of lower extremity kinematics during level walking. *Journal of Orthopaedic Research* 8(3): 383–392.

Kawamoto H, Kanbe S and Sankai Y (2003) Power assist method for HAL-3 using EMG-based feedback controller. In: *IEEE international conference on systems, man and cybernetics*, pp. 1648–1653.

Kazerooni H and Steger R (2006) The Berkeley Lower Extremity Exoskeleton. *Journal of Dynamic Systems, Measurement, and Control* 128(1): 14.

Kim DH, Ghaffari R, Lu N, et al. (2012) Electronic sensor and actuator webs for large-area complex geometry cardiac mapping and therapy. *Proceedings of the National Academy of Sciences of the United States of America* 109(49): 19910–19915.

Kim DH, Lu N, Ma R, et al. (2011) Epidermal electronics. *Science* 333(6044): 838–843.

Kong K and Jeon D (2006) Design and control of an exoskeleton for the elderly and patients. *IEEE/ASME Transactions on Mechatronics* 11(4): 428–432.

Kramer RK, Majidi C, Sahai R and Wood RJ (2011) Soft curvature sensors for joint angle proprioception. In: *IEEE/RSJ international conference on intelligent robots and systems*, pp. 1919–1926.

Legnani G, Zappa B, Casolo F, Adamini R and Magnani PL (2000) A model of an electro-goniometer and its calibration for biomechanical applications. *Medical Engineering and Physics* 22(10): 711–722.

Lipomi DJ, Vosgueritchian M, Tee BCK, et al. (2011) Skin-like pressure and strain sensors based on transparent elastic films of carbon nanotubes. *Nature Nanotechnology* 6(12): 788–792.

Lu TW and O'Connor JJ (1999) Bone position estimation from skin marker co-ordinates using global optimisation with joint constraints. *Journal of Biomechanics* 32(2): 129–134.

Luinge HJ and Veltink PH (2005) Measuring orientation of human body segments using miniature gyroscopes and accelerometers. *Medical and Biological Engineering and Computing* 43(2): 273–282.

Majidi C, Kramer RK and Wood RJ (2011) A non-differential elastomer curvature sensor for softer-than-skin electronics. *Smart Materials and Structures* 20(10): 105017.

Makinson BJ (1971) *Research and Development Prototype for Machine Augmentation of Human Strength and Endurance. Hardiman I Project*. Technical Report 196, Specialty Materials Handling Products Operation, General Electric Co, Schenectady, NY, USA.

Mengüç Y, Park YL, Martinez-Villalpando E, et al. (2013) Soft wearable motion sensing suit for lower limb biomechanics measurements. In: *IEEE international conference on robotics and automation*, pp. 5289–5296.

Messler RW (2004) *Joining of Materials and Structures: From Pragmatic Process to Enabling Technology,* 1st edn. Burlington, MA: Elsevier.

Meyers MA and Chawla KK (2008) *Mechanical Behavior of Materials,* 2nd edn. Cambridge, UK: Cambridge University Press.

Miserez A, Schneberk T, Sun C, Zok FW and Waite JH (2008) The transition from stiff to compliant materials in squid beaks. *Science* 319(5871): 1816–1819.

Park YL, Chen BR, Pérez-Arancibia NO, et al. (2014) Design and control of a bio-inspired soft wearable robotic device for ankle–foot rehabilitation. *Bioinspiration and Biomimetics* 9(1): 016007.

Park YL, Chen BR and Wood RJ (2012) Design and fabrication of soft artificial skin using embedded microchannels and liquid conductors. *IEEE Sensors Journal* 12(8): 2711–2718.

Park YL, Chen Br, Young D, et al. (2011) Bio-inspired active soft orthotic device for ankle foot pathologies. In: *IEEE/RSJ international conference on intelligent robots and systems*, pp. 4488–4495.

Park YL, Majidi C, Kramer RK, Bérard P and Wood RJ (2010) Hyperelastic pressure sensing with a liquid-embedded elastomer. *Journal of Micromechanics and Microengineering* 20(12): 125029.

Pratt J, Krupp B, Morse C and Collins S (2004) The RoboKnee: an exoskeleton for enhancing strength and endurance during walking. In: *IEEE international conference on robotics and automation*, pp. 2430–2435.

Qi HJ, Joyce K and Boyce MC (2003) Durometer hardness and the stress–strain behavior of elastomeric materials. *Rubber Chemistry and Technology* 76(2): 419–435.

Ramuz M, Tee BCK, Tok JBH and Bao Z (2012) Transparent, optical, pressure-sensitive artificial skin for large-area stretchable electronics. *Advanced Materials* 24(24): 3223–3227.

Rogers JA, Someya T and Huang Y (2010) Materials and mechanics for stretchable electronics. *Science* 327(5973): 1603–7.

Shulte JrHF (1961) The characteristics of the McKibben artificial muscle. In: *The Application of External Power in Prosthetics and Orthotics; A Report*. Washington, DC: National Academy of Sciences - National Research Council.

Tao Y, Hu H and Zhou H (2007) Integration of vision and inertial sensors for 3D arm motion tracking in home-based rehabilitation. *The International Journal of Robotics Research* 26(6): 607–624.

Tesconi M, Tognetti A, Scilingo EP, et al. (2007) Wearable sensorized system for analyzing the lower limb movement during rowing activity. In: *IEEE international symposium on industrial electronics*, pp. 2793–2796.

Tognetti A, Carbonaro N, Zupone G and De Rossi D (2006) Characterization of a novel data glove based on textile integrated sensors. In: *IEEE engineering in medicine and biology society annual international conference*, pp. 2510–2513.

Tsuji T, Momiki C and Sakaino S (2013) Stiffness control of a pneumatic rehabilitation robot for exercise therapy with multiple stages. In: *2013 IEEE/RSJ international conference on intelligent robots and systems. IEEE*, pp. 1480–1485.

van Sint Jan S (2007) *Color Atlas of Skeletal Landmark Definitions: Guidelines for Reproducible Manual and Virtual Palpations,* 1st edn. Philadelphia, PA: Elsevier.

Viventi J, Kim DH, Vigeland L, et al. (2011) Flexible, foldable, actively multiplexed, high-density electrode array for mapping brain activity in vivo. *Nature Neuroscience* 14(12): 1599–605.

Vogt DM, Park YL and Wood RJ (2013) Design and characterization of a soft multi-axis force sensor using embedded microfluidic channels. *IEEE Sensors Journal* 13(10): 4056–4064.

Walsh CJ, Endo K and Herr H (2007) A quasi-passive leg exoskeleton for load-carrying augmentation. *International Journal of Humanoid Robotics* 4(3): 487–506.

Wehner M, Quinlivan B, Aubin PM, et al. (2013) A lightweight soft exosuit for gait assistance. In: *IEEE international conference on robotics and automation*, pp. 3347–3354.

Whitesides GM (2006) The origins and the future of microfluidics. *Nature* 442(7101): 368–373.

Winter DA (1984) Kinematic and kinetic patterns in human gait: Variability and compensating effects. *Human Movement Science* 3(1–2): 51–76.

Winter DA (1990) *Biomechanics and Motor Control of Human Movement,* 1st edn. New York, NY: John Wiley & Sons.

Wise S, Gardner W, Sabelman E, et al. (1990) Evaluation of a fiber optic glove for semi-automated goniometric measurements. *The Journal of Rehabilitation Research and Development* 27(4): 411.

Xia Y and Whitesides GM (1998) Soft lithography. *Annual Review of Materials Science* 28(1): 153–184.

Yagn N (1890) Apparatus for facilitating walking, running, and jumping. US Patent No. 420179.

Yamada T, Hayamizu Y, Yamamoto Y, et al. (2011) A stretchable carbon nanotube strain sensor for human-motion detection. *Nature Nanotechnology* 6(5): 296–301.

Yamamoto K, Ishii M, Hyodo K, Yoshimitsu T and Matsuo T (2003) Development of power assisting suit (miniaturization of supply system to realize wearable suit). *JSME International Journal Series C* 46(3): 923–930.

Yifan DL and Hsiao-Wecksler ET (2013) Gait mode recognition and control for a portable-powered ankle–foot orthosis. In: *IEEE international conference on rehabilitation robotics*, pp. 1–8.

Yun X and Bachmann ER (2006) Design, implementation, and experimental results of a quaternion-based Kalman filter for human body motion tracking. *IEEE Transactions on Robotics* 22(6): 1216–1227.

Zhang R, Deng H, Valenca R, et al. (2012) Carbon nanotube polymer coatings for textile yarns with good strain sensing capability. *Sensors and Actuators A: Physical* 179: 83–91.

Zhou H and Hu H (2008) Human motion tracking for rehabilitation – a survey. *Biomedical Signal Processing and Control* 3(1): 1–18.